

Initial Results on SiPM Performance for use in Medical Imaging

Nikos Efthimiou, Giannis Argyropoulos
and George Panayiotakis
Medical Physics dep.
Univ. of Patras
Patras, Greece
Email:panayiot@upatras.gr

Nikos Efthimiou
Inst. of Radioisotopes-
Radiodiagnostic Products,
N. C. S. R. Demokritos,
Athens, Greece
Email:efthimioun@upatras.gr

Maria Georgiou, George Loudos
Medical Instruments dep.
Technological Educational Inst. of Athens
Athens,Greece
Email:gloudos@teiath.gr

Abstract—Silicon Photomultiplier (SiPM) detectors are attractive candidates for the replacement of Photomultipliers in nuclear imaging. They are compact, provide high gain with low V_{bias} and have fast response. In addition, SiPMs are not influenced by strong magnetic fields, allowing the use in the emerging field of PET-MRI. The development of small prototypes based on SiPMs poses several design challenges, since it is necessary to optimize scintillator and SiPM coupling, as well as signal amplification and digitization. In this work, we investigated the performance of 3 simple SiPM modules constructed by SensL corporation coupled on various scintillator detectors, suitable for SPECT and PET systems. ^{99m}Tc , ^{111}In and ^{18}F were used. The readout system includes the SensL preamplifier circuit, a nuclear imaging module (NIM) amplifier and analog to digital converter (ADC) controlled by MPA/WIN (Multiparameter Analyser) software. The parameters that have been measured are: output pulse shape, dark count rate (DCR), detection efficiency, linearity and energy resolution for different bias voltages (V_{bias}) and photon energies. Best energy resolution was experimentally measured 11% for 511keV and 23% for 140keV. V_{bias} applied on SiPMs strongly affects output pulse amplitude and depends on the SiPM characteristics.

I. INTRODUCTION

The typical structure of a silicon photomultiplier (SiPM) is built on a 3-5 μm thick lowly doped p-type epitaxial layer π which was grown on a highly doped p-type substrate (p+). The abrupt junction is obtained by creating an n+ zone on the superficial region of the epitaxial layer. Usually, a second p-type region is created underneath the n+ to x the breakdown voltage to the desired value. Thus, the complete structure, from top to bottom, is n+ / p / p / p+. A SiPM structure correlates to a matrix aggregated by multiple rows of diodes coupled to a resistor [1]. Detailed description of the SiPM engineering has been previously published by Brian F. Aull et. al. [1]. This construction method leads to poor detection efficiency below blue light [2], [3]. Several groups have proposed alternative schemes which enhance blue light sensitivity [2].

Although a commercial imaging system based on SiPMs detectors has not been presented yet, a number of research prototypes have been developed both for experimental [3]-[5] and preliminary imaging purposes [6]. At the moment conventional scintillators such as LYSO, NaI(Tl) and CsI(Tl) have been assessed by many groups [5].

The aim of this paper is the characterisation of three SiPM modules when different scintillator materials and different radioactive sources were used. We assess the performance of LSO:Ce, GSO:Ce, GSO:Zr,Ce and LGSO:Ce single crystal fast scintillators, which have been already used in nuclear medicine. Pulse characteristics, which are essential for the design of the readout system are given as a function of V_{bias} , scintillator material and source energy.

II. MATERIALS AND METHODS

The SiPMs that were tested are included in SensL's Scint-Pack evaluation package. SPMMicro3020X13 and SPMMicro3035X13 have an overall area of 3x3mm, with 20 μm and 35 μm pixels respectively. The SPMMicro6035X13 has an overall area of 6x6mm, with 35 μm pixels. Detailed specifications of SiPMs can be found in manufacturer's datasheets [7]. The scintillators that were used in SiPMs evaluation are summarized in Table I.

TABLE I
SCINTILLATION CRYSTALS CHARACTERISTICS

Material	Dimensions	Provider
BGO	3x3x15mm ³	SensL
LYSO:Ce	3x3x15mm ³	SensL
CsI:Tl	3x3x15mm ³	SensL
CsI:Tl	6x6x30mm ³	SensL
LSO:Ce	10x10x10mm ³	Siemens CTI
GSO:Ce	10x10x10mm ³	Hitachi Chem.
GSO:Zr,Ce	5x5x20mm ³	Hitachi Chem.
LGSO:Ce	5x5x20mm ³	Hitachi Chem.

A. Output Pulse Characteristics

The pulse characteristics (amplitude and the width) after the preamplification stage, have been recorded. ^{99m}Tc and ^{111}In sources were used for excitation. Pulse characteristics were measured using an Agilent DSO1022A oscilloscope. 16 pulses were summed and their average value was used. This measured data provide useful information for the selection of amplification and digitization components of the rest of the data acquisition (DAQ) system.

B. Dark Count Rate (DCR)

To measure the dark count rate, the preamplified output of the SiPMs was connected to a ORTEC 772 NIM discriminator and the generated pulses to a LRS 621 NIM counter without the use of a radioactive source. The V_{bias} plays a major role to the portion of DCR recorded by the system due to thermally generated electrons. DCR increases with temperature, detector volume and V_{bias} .

C. Estimation of Scintillation Signal

The photon detection efficiency (PDE) is the statistical probability that an incident photon produces a Geiger avalanche from one of the single photon avalanche detectors (SPAD). PDE depends on (a) intrinsic quantum efficiency of silicon (b) the geometrical active area and (c) the probability of initializing an avalanche. The first two factors are fixed for a particular device but the third varies as a function of V_{bias} [8].

The signal was amplified using an ORTEC 570 spectroscopic amplifier, and digitized using FastComTech 7070 ADC and MPA/WIN software, with 12bit resolution and 2048 channels. However, the particular amplifier is not capable of amplifying fast signals obtained from GSO, LYSO and most of the scintillators included in this study. Thus the relative PDE (\overline{PDE}), of the three SiPMs was evaluated for the combination of CSI:Tl with the three SiPMs.

In order to perform \overline{PDE} calculation we used formula 1 [10].

$$\overline{PDE} = \frac{\int E_{scint}(\lambda) \times PDE(\lambda) d\lambda}{\int E_{scint}(\lambda) d\lambda} \quad (1)$$

The number of photoelectrons (N_{PE}) was calculated by formula 2 with the use of the quantum detection efficiency (QDE) [9] which adds the efficiency of the crystal to our model and the use of PDE in the place of quantum efficiency (QE) [10], which characterises better SiPM:

$$N_{P.E.} = \Psi \times \overline{PDE} \times LCE \times E_{\gamma} \times QDE \quad (2)$$

where Ψ is the scintillator's light yield, LCE is the light collection efficiency and E_{γ} is the gamma photon energy.

D. Linearity

In order to estimate the linearity, of the detector module consting of CSI:Tl coupled on SiPM, we measured the ADC channels where energy spectrum peaks for different V_{bias} . In addition we calculated $N_{P.E.}$ for the same voltages.

E. Energy Resolution

Energy resolution (R) is a straightforward measure of the ability of the detector to distinguish between gamma rays of different energies. It is expressed as a percentage and it is equal to the photopeak full width at half maximum (FWHM) divided by the photopeak center energy (P). Energy resolution is affected by the characteristics of both the scintillator and SiPMs as well as counting statistics. FWHM values were

extracted multiplying by 2.354 times the variance of the distribution σ .

$$R = \frac{FWHM(ch)}{P(ch)} \times 100 \quad (3)$$

III. RESULTS AND DISCUSSION

A. Pulse Characteristics

In Fig. 1 three pulses of the SPMMicro3020 with V_{bias} at 32V using ^{99m}Tc - CSI:Tl, ("Fig." 1(a)), BGO ("Fig." 1(b)) and LYSO:Ce ("Fig." 1(c)) - were obtained.

In Tables II, III and IV are summarized the amplitude and the width of the output pulses from the three SiPMs at different V_{bias} , scintillation crystals and irradiation sources (^{99m}Tc and ^{111}In). The amplitude of the pulses increases as V_{bias} takes higher values, due to the increased gain and the greater photon detection propability of optical photons. SPMMicro3035 contains larger cells, $35\mu m$ and has higher amplitude pulses due to their higher capacitance properties [11]. Furthermore, increased V_{bias} leads to wider pulses, since the RC constant is higher. Measurements were conducted under approximately $40^{\circ}C$.

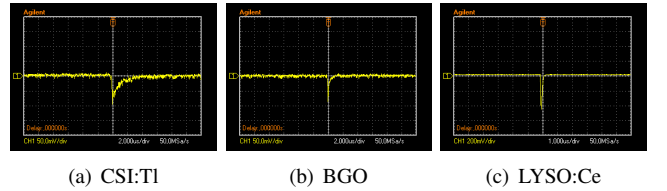


Fig. 1. SPMMicro3020 pulses for 32V V_{bias} and three different scintillation

TABLE II
AVERAGE PULSE SIZE OF EACH SPMMICRO FOR DIFFERENT V_{bias} AND CRYSTALS (SENSL EVALUATION PACK) USING ^{99m}Tc ISOTOPE

Crystal	V_{bias} (V)	SPMM3020		SPMM3035		SPMM6035	
		(mV)	(μsec)	(mV)	(μsec)	(mV)	(μsec)
BGO	29	-	-	15	1.50	10	0.9
	30	30	0.85	30	1.00	20	0.9
	31	75	0.60	70	1.2	70	0.8
	32	80	0.40	110	1	100	0.7
CSI:Tl	29	6	4.00	32	6	40	4.5
	30	45	0.40	60	4.5	80	5
	31	60	3.20	100	5.5	140	4.0
	32	100	3.00	220	5	200	3
LYSO:Ce	29	70	0.40	70	0.5	400	0.6
	30	80	0.32	200	0.4	600	0.5
	31	180	0.30	400	0.35	1000	0.4
	32	400	0.20	1000	0.4	1100	0.35

B. Dark Count Rate - DCR

Fig. 2 illustrates the DCR results of SPMMicro3020 and SPMMicro3035 for applied V_{bias} equal to 32V. Due to the high applied V_{bias} each SPAD has a significant probability to initiate an avalanche breakdown due to thermally generated electrons.

SPMMicro3035 demonstrates greater DCR values than SPMMicro3020 for the corresponding V_{bias} . The optimum

TABLE III
AVERAGE PULSE SIZE OF EACH SPMMICRO FOR DIFFERENT V_{bias} AND CRYSTALS USING ^{99m}Tc ISOTOPE

Crystal	V_{bias} (V)	SPMM3020		SPMM3035		SPMM6035	
		(mV)	(μ sec)	(mV)	(μ sec)	(mV)	(μ sec)
LSO:Ce	29	50	0.30	30	0.20	200	0.30
	30	200	0.30	150	0.20	400	0.30
	31	200	0.25	200	0.20	500	0.25
	32	450	0.20	500	0.20	600	0.25
GSO:Ce	29	10	0.20	6	0.30	15	0.20
	30	20	0.20	20	0.40	20	0.15
	31	40	0.20	50	0.40	50	0.15
	32	100	0.30	150	0.20	150	0.30
GSO:Zr,Ce	29	20	0.20	10	0.10	20	0.20
	30	50	0.20	40	0.20	50	0.20
	31	80	0.20	100	0.15	100	0.20
	32	150	0.30	200	0.20	200	0.30
LGSO:Ce	29	100	0.20	30	0.20	100	0.20
	30	200	0.20	100	0.20	200	0.30
	31	200	0.20	200	0.10	500	0.25
	32	250	0.30	500	0.20	600	0.30

TABLE IV
AVERAGE PULSE SIZE OF EACH SPMMICRO FOR DIFFERENT V_{bias} AND CRYSTALS USING ^{111}In ISOTOPE

Crystal	V_{bias} (V)	SPMM3020		SPMM3035		SPMM6035	
		(mV)	(μ sec)	(mV)	(μ sec)	(mV)	(μ sec)
BGO	29	-	-	-	-	-	-
	30	-	-	-	-	-	-
	31	-	-	-	-	-	-
	32	150	0.80	120	1.60	-	-
CSI:Tl	29	60	5.00	20	2.40	-	-
	30	240	-	44	2.00	125	2.50
	31	300	4.00	120	2.00	250	2.20
	32	300	2.40	300	2.00	220	2.40
LYSO	29	170	0.32	100	0.24	-	-
	30	400	0.30	240	0.20	-	-
	31	900	0.32	760	0.20	-	-
	32	1010	0.28	-	0.20	-	-

V_{bias} threshold for SPMMicro3020 was $0.5mV$ and for SPMMicro3035 was $1mV$. These thresholds ensures dark count rate lower than 1 count per second.

C. Detection Efficiency and linearity at different V_{bias} .

QDE of CSI:Tl for ^{99m}Tc was found, according to [9], equal to 0.997. LCE is assumed to be equal to 40% following

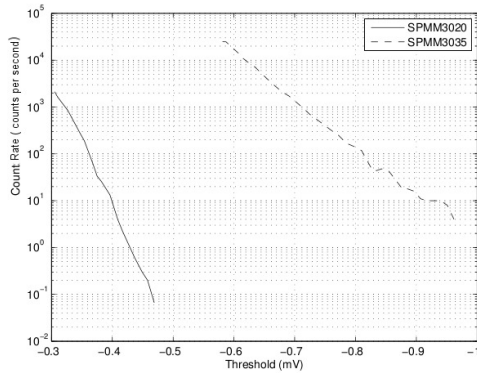


Fig. 2. DCR of the two SiPMs for different threshold levels

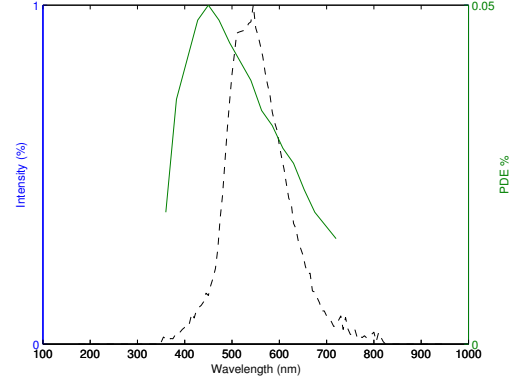


Fig. 3. CSI:Tl normalised emission spectrum and PDE as a function of wavelength

the assumption of publication [8]. For \overline{PDE} calculation we use the formula 1 and absolute PDE curve and the normalized CSI:Tl emission spectrum, as shown in Fig. 3.

The calculated N_{PE} as well as the channel where the emission peak appears, are displayed on Fig. 4(a) and 4(b), for SPMMicro3020 and SPMMicro3035, respectively. The detection efficiency in terms of N_{PE} is found to increase significantly, between bias values of 29V and 32V for SPMMicro3020 (a factor of 2) for SPMMicro3035 (a factor of 2.5). SPMMicro3020 after 30.5V demonstrates a deviation from linearity mainly to the increased noise contribution.

For SPMMicro3035 the linearity is observed until 30 V_{bias} . The slightly lower voltage value of SPMMicro3035 compared to SPMMicro3020 may be explained due to its smaller capability to detect a large number of photons.

D. Energy Resolution at Different Energies

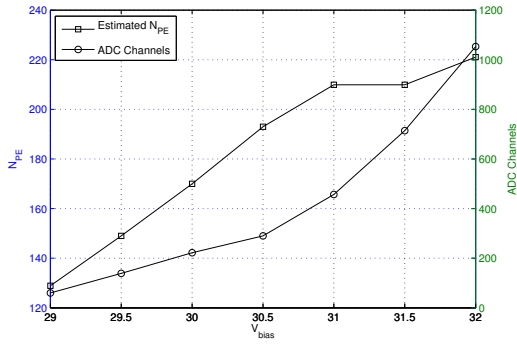
The calculated energy resolutions are summarized at Table V. Energy resolution, as expected, was improved in greater energies. SPMMicro3035 provided best energy resolution in all cases compared with the other two. Measured energy resolution values were 23%, 20% and 11% for ^{99m}Tc , ^{111}In and ^{18}F , respectively. SPMMicro3020 provided corresponding values of 25.3%, 27% and 14%.

TABLE V
ENERGY RESOLUTION AT DIFFERENT ENERGIES, FOR 30 V_{bias} USING CSI:Tl

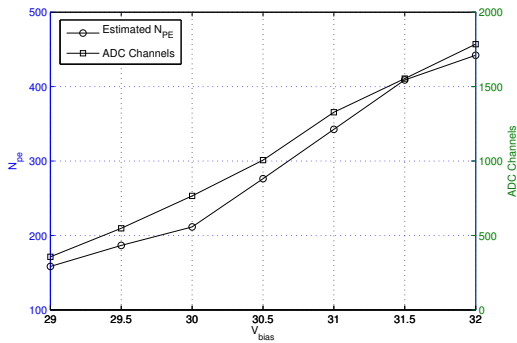
Energy (keV)	SPMM3020	SPMM3035	SPMM6035
140	25%	23%	35%
171	27%	20%	35%
245	21%	17%	30%
511	14%	11%	13%

E. Energy Resolution at different V_{bias}

Energy resolution was measured for CSI:Tl and ^{99m}Tc produced gamma rays at 30 V_{bias} . A Gaussian fit was applied on the acquired raw spectrum data and energy resolution values were calculated using formula 3. Normalized energy



(a) SPMMicro3020



(b) SPMMicro3035

Fig. 4. Estimated N_{PE} (left axis), ADC Channels (right axis) of ^{99m}Tc photopeak for different V_{bias}

spectra from the SiPMs for seven different V_{bias} are shown on Fig. 5(a) and Fig. 5(b).

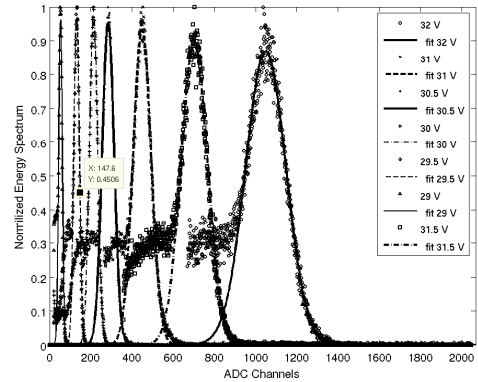
Energy resolution values are shown in Table VI. Bias voltage improve energy resolution until 31V due the improved PDE.

TABLE VI
ENERGY RESOLUTIONS AT DIFFERENT V_{bias}

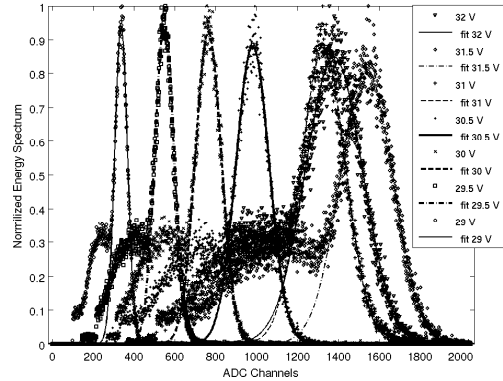
V_{bias}	SPMM3020	SPMM3035	SPMM6035
29V	30%	24%	38%
29.5V	26%	24%	37%
30V	25%	23%	35%
30.5V	24%	19%	30%
31V	23%	19%	28%
31.5V	22%	19%	28%
32V	22%	19%	28%

IV. CONCLUSIONS AND FUTURE WORK

The presented results demonstrate that during the design and optimization of an imaging system based on SiPMs several parameters have to be taken into account. Depending on the scintillator material used, the amplitude and timing characteristics of output pulses significantly affect the amplification and digitization circuit. New SiPMs show optimized efficiency in lower wavelengths. However, a number of scintillators have an output in higher wavelengths and the total systems efficiency needs to be investigated. Small changes in V_{bias} affect pulse



(a) SPMMicro3020



(b) SPMMicro3035

Fig. 5. Energy spectra of $CsI : Tl$ scintillation crystal excited by ^{99m}Tc at different V_{bias}

characteristics as well as energy resolution. In addition, energy resolution is affected by sources energy; thus if a system is intended for only SPECT or PET imaging, this can lead to different setting in V_{bias} .

The shape of all spectra, when various crystals were tested, was similar to the one theoretically expected. However, the comparison of CsI, and LYSO spectra showed that in the later case there is a shift towards lower channels, although higher light output is expected. The light pulse duration of LYSO is very fast and this implied that the amplifier did not properly follow input signals and only part of the pulse was finally amplified. So, a carefully selection of DAQ components has to be carried out for acquisition of fast pulses. At the moment, we are designing a new amplification board based on AD8001, which is suitable for fast signals with careful selection of fast DAQ components. In addition, signals have already been digitized using a FPGA system based on Spartan 3E. A new FPGA based system is being implemented, since the results of this work demonstrate that a fast sampling rate ADC is also necessary for efficient signal digitization.

ACKNOWLEDGMENT

The research leading to these results has received funding from the European Community's Seventh Framework Program (FP7/2007-2013) under grant agreement Number 201380. We specially thank Prof. Valais Giannis and Dr. David Stratos, from the department of Medical Instruments Technology of the Technical Educational Inst. of Athens for lending us their equipment and sharing their precious time and knowledge.

REFERENCES

- [1] B.F. Aull, A.H. Loomis, D.J. Young, R.M. Heinrichs, B.J. Felton, P.J. Daniels and D.J. Landers, "Geiger-Mode Avalanche Photodiodes for Three-Dimensional Imaging", Vol.13, *Lincoln Laboratory*, 2002.
- [2] C. Piemonte, "A new Silicon Photomultiplier structure for blue light detection", *Nucl. Instrum. Meth. Phys. A.*, Vol.568, pp.224-232, 2006.
- [3] G. Llosa, N. Belcari, M.G. Bisogni, G. Collazuol, S. Marcatili, S. Mochrs, F. Morsani, C. Piemonte and A. Del Guerra, "Energy and Timing Resolution Studies With Silicon Photomultipliers (SiPMs) and 4-Pixel SiPM Matrices for PET", *IEEE Trans. on Nucl. Sci.*, Vol.56, pp.543-548, 2009.
- [4] R. Hawkes, A. Lucas, J. Stevick, G. Llosa, S. Marcatili, C. Piemonte, A. Del Guerra, T.A. Carpenter, "Silicon Photomultiplier Performance Tests in Magnetic Resonance Pulsed Fields", *IEEE Nucl. Sci. Symp. Conf. Record*, pp.1082-3654, 2007.
- [5] P.S. Marrocchesi, M.G. Bagliesi, K. Batkov, G. Bigongiari, M.Y. Kim, T. Lomtadze, P. Maestro, F. Morsani, R. Zei "Active control of the gain of a 3 mm Silicon PhotoMultiplier", *Nucl. Instrum. Meth. A.*, Vol.602, pp.391-395, 2009.
- [6] S. Majewski, J. Proffitt, J. McKisson, R. Raylman, A. Stolin and A.G. Weisenberger "Initial Tests of a Compact Imaging Photomultiplier Made From Array of $3 \times 3 \text{ mm}^2$ Hamamatsu MPPC-SMD Modules" available online www.iss.infn.it/garibaldi/temp/NSSSiPm-majewski-paper.pdf.
- [7] SensL corp. SPMMicro datasheet Rev. Jan-10 [Online]. Available: <http://sensl.com/resource-centre/datasheets/>
- [8] D.J. Herbert, V. Saveliev, N. Belcari, N. D'Ascenzo, A. Del Guerra and A. Golovin "First Results of Scintillator Readout With Silicon Photomultiplier", *IEEE Trans. on Nucl. Sci.*, Vol.53, 2006
- [9] S. David, C. Michail, M. Roussou, E. Nirgianaki, A. Toutountzis, I. Valais, G. Fountos, I. Kandarakis, G. Panagiotakis "Evaluation of the luminescence efficiency of YAG:Ce powder scintillating screens for use in digital mammography detectors", *IEEE NSS*, pp.3950-3959, 2008.
- [10] D.J. Herbert, V. Saveliev, N. Belcari, N. D'Ascenzo, A. Del Guerra, A. Golovin "First Results of Scintillator Readout with Silicon Photomultiplier", *IEEE Trans. on Nucl. Sci.*, Vol.53, pp.389-394, 2006.
- [11] V. Golovina, V. Saveliev. "Novel type of avalanche photodetector with Geiger mode operation". *Nucl. Instrum. Meth. A.*, Vol.518, pp.560-564, 2004.